Catalysis Science & Technology

Accepted Manuscript

This is an *Accepted Manuscript*, which has been through the RSC Publishing peer review process and has been accepted for publication.

Accepted Manuscripts are published online shortly after acceptance, which is prior to technical editing, formatting and proof reading. This free service from RSC Publishing allows authors to make their results available to the community, in citable form, before publication of the edited article. This *Accepted Manuscript* will be replaced by the edited and formatted *Advance Article* as soon as this is available.

To cite this manuscript please use its permanent Digital Object Identifier (DOI®), which is identical for all formats of publication.

More information about *Accepted Manuscripts* can be found in the **Information for Authors**.

Please note that technical editing may introduce minor changes to the text and/or graphics contained in the manuscript submitted by the author(s) which may alter content, and that the standard **Terms & Conditions** and the **ethical guidelines** that apply to the journal are still applicable. In no event shall the RSC be held responsible for any errors or omissions in these *Accepted Manuscript* manuscripts or any consequences arising from the use of any information contained in them.

Catalysis Science & Technology RSCPublishing

ARTICLE

The role of surface Zn^{2+} ions in the transesterification of vegetable oils over ZnO supported on Al_2O_3 and Fe_2O_3

Cite this: DOI: 10.1039/xoxxoooooox

Received ooth January 2012,
Accepted ooth January 2012

DOI: 10.1039/xoxxoooooox

www.rsc.org/

K. Thirunavukkarasu*,[a] T.M. Sankaranarayanan[a, b], A. Pandurangan[b], R. Vijaya Shanthi[a] and S. Sivasanker[a],

Samples of $ZnO-Al_2O_3$ and $ZnO-Fe_2O_3$ with different loadings of ZnO (5 – 20 wt%) were prepared by impregnation of the supports (γ-Al_2O_3 and α-Fe_2O_3) with $ZnNO_3$ and calcining at 873 K. XRD of the calcined samples revealed that the ZnO had reacted with the support to form the corresponding spinels, $ZnAl_2O_4$ and $ZnFe_2O_4$. The catalytic activity of the supported spinel samples, and samples of stoichiometric $ZnAl_2O_4$ and $ZnFe_2O_4$ prepared by co-precipitation were examined for the transesterification of sunflower, waste cooking oil and jatropha oil. A linear relationship between the spinel content, estimated by XRD, and surface Zn concentration estimated by XPS and transesterification activity of the samples is obtained. XVB (x-ray valence band) studies provide evidence to suggest that Zn 3d electrons may take part to a major extent in the electronic excitation of the spinels ($ZnAl_2O_4$ and $ZnFe_2O_4$) and, presumably, their catalytic activity..

1. Introduction:

Fatty acid methyl esters (FAME; biodiesel), the key product of transesterification of vegetable oils, are among the important renewable transportation fuels in use today. Their increased use is expected to decrease the rate of CO_2 build up in the atmosphere. The transesterification of vegetable oils is at present mostly carried out using soluble alkali catalysts. The disadvantages of using alkali catalysts are soap formation, poor quality of byproduct glycerol, wastewater generation and non-suitability for oils containing free fatty acids (FFA). Though many solid catalysts were reported[1-5] as alternative for the homogeneous acid catalyst, a $ZnAl_2O_4$ based catalyst was developed for transesterification by the Institut Francais du Petrole (IFP) and was commercialized by Axens[6,7].

$ZnAl_2O_4$ belongs to AB_2O_4 spinel oxides and possess good thermal stability, no/least leaching during reactions, hydrophobicity and ease of preparation with large external areas. Apart from transesterification, $ZnAl_2O_4$ is known to be active as a heterogeneous catalyst for reactions like dehydration, hydrogenation, dehydrogenation, cracking, synthesis of fine chemicals[8-13] and in photocatalytic reactions[14,15]. $ZnFe_2O_4$, another important candidate in the AB_2O_4 spinel oxides, is reported to be active heterogeneous catalyst for N-alkylation reactions[16,17], water gas shift reaction[18], O-acylation[19], and oxidative dehydrogenation n-butane[20,21], and as a photocatalyst for water splitting reactions[22], decomposition of organic pollutants[23] and hydrogen production[24]. In AB_2O_4 spinel oxides, more of octahedral sites are exposed on the surface than the tetrahedral sites according to Low Energy Ion Scattering (LEIS) studies[25,26], i.e., more B atoms are present in the surface than A atoms.

After Axens process, many reports on $ZnAl_2O_4$ catalysts for transesterification of vegetable oils started to emerge in the literature[27-31]. Many of them mainly deal with the engineering aspects of the process and reveal the importance of large surface area and pores. Jiang et al[29] observed that the transesterification reaction on Zn/Al mixed oxide catalysts was more feasible due to its basic sites. Liu et al[30] reported that strong basicity and large pores were beneficial for the La-loaded $ZnAl_2O_4$ catalysed transesterification reaction. They found that La-loading of 5.5 wt% showed highest activity though they had strongly basic catalysts with higher La-loadings. To contradict these studies, a recent literature report on transesterification reaction reveals that $ZnAl_2O_4$ surface contains more acidic sites than basic sites[31].

Interaction of ZnO with the γ-Al_2O_3 or α-Fe_2O_3 supports is reported in the literature. Strohmeier and Hercules[32] observed that Zn^{2+} ions interact strongly with γ-Al_2O_3 support for >20%

loadings of ZnO to form surface spinels. An electronic interaction between Zn^{2+} and Fe^{3+} ions of $ZnFe_2O_4$-ZnO catalysts was observed through Mossbauer spectroscopy by Armendariz et al[21] though Zn^{2+} ions were not involved directly in the oxidative dehydrogenation reaction of n-butane. Unfortunately, the authors could not find the same with Fe_2O_3-$ZnFe_2O_4$ catalysts as Zn is inactive in Mossbauer spectroscopy. The role of Zn ions in the spinel catalysis is recognised in the following studies. Sreekumar et al studied alkylation reactions Zn-Co mixed ferrites and observed that the catalyst with a ratio with more Zn^{2+} content is more active and selective for the N-methylation reaction of aniline[17]. Vijayaraj et al[16] observed an active spacer role of Zn^{2+} ions for the N-methylation reaction on Zn-Cu mixed ferrites and stabilizing Cu^{2+} ions during reaction by Zn^{2+} from XPS studies.

We now present our studies on the catalytic activity of ZnO supported on γ-Al_2O_3 and α-Fe_2O_3 in the transesterification of vegetable oils, viz. sunflower oil, waste (used) sunflower oil and jatropha oil, carried out as part of our ongoing research on the transesterification of vegetable oils with solid oxide catalysts and spinel oxides[33,34]. Samples of ZnO/Al_2O_3 and ZnO/Al_2O_3 containing different amounts of ZnO were prepared by impregnation, characterized by physicochemical methods and their activity for the transesterification with methanol of sunflower oil, waste cooking oil and jatropha oil were evaluated in a batch reactor. XPS studies reveal the active role of Zn-ions in the transesterification reactions.

2. Experimental Section

2.1. Materials used and preparation of catalysts

Cooking grade sunflower oil, waste (used) sunflower oil and jatropha oil were procured locally. Their fatty acid compositions are reported in Table 1. Methanol (AR Grade; SRL, India) was distilled and dried over molecular sieve (4 Å) prior to use.

Table 1 Composition of the vegetable oils.

Fatty acid composition [%]	Sunflower oil	Waste cooking oil	Jatropha oil
Palmitic acid (C16:0)	6.5	6.3	17.9
Stearic acid (C18:0)	0.5	0.5	7.3
Oleic acid (C18:1)	22.5	21.9	41.8
Linoleic acid (C18:2)	70.5	68.8	25.0
Free Fatty acids (FFA)	-	2.5 / [C_{16}, 0.2; $C_{18:1}$, 0.9; $C_{18:2}$, 1.4]	8.0 / [C_{16}, 2.0; $C_{18:1}$, 3.2; $C_{18:2}$, 2.4; C_{18}, 0.4]

Samples of ZnO-Al_2O_3 and ZnO-Fe_2O_3 with different loadings of ZnO (5 – 20 wt%) were prepared by impregnation of the supports (γ-Al2O3 and α-Fe2O3) with $ZnNO_3$, drying in air (353 K; 12 h) and calcining at 873 K (6 h). Additionally, the spinels $ZnAl_2O_4$ and $ZnFe_2O_4$ were prepared by mixing stoichiometric amounts of the required metal nitrate solutions (1:2 mole ratio; 40 ml) and adding rapidly to a solution of NH_4OH (25 wt%; vol. 25 ml) at room temperature (300 K) under constant and vigorous stirring. The precipitates were aged for 12 hours and dried at 353 K in an air oven for about 12 hours. The dried materials were powdered and calcined at 873 K for 6 h. The stoichiometric spinels are represented by the general formula ZnB_2O_4, where B is Al or Fe, and the non-stoichiometric mixed oxides are represented by nZnB, where n represents wt% of ZnO loading in the support.

2.2. Characterization of supports and catalysts

X-ray diffraction (XRD) patterns of the calcined materials were obtained using a Rigaku Miniflex II with Cu Kα radiation. The phases were identified by matching of the peaks with JCPDS (Joint Committee on Powder Diffraction Standards) data files. Surface area determination was performed by the BET method (Micromeritics ASAP 2020). Before analysis the samples were degassed at 623 K for 8 to 10 h. The acidity of the samples was measured by temperature-programmed desorption (TPD) of ammonia (AutoChem 2910, Micromeritics, USA). The standard procedure for the TPD measurements involved the activation of the sample in flowing He at 873 K (1 h), cooling to 323 K, adsorbing NH_3 from a He-NH_3 (10 %) mixture, desorbing in He at 323 K for 30 min, and finally carrying out the TPD experiment by raising the temperature of the catalyst in a programmed manner (10 K min^{-1}). The areas under the TPD curves were converted into meq NH_3 per gram of catalyst based on injection of known volumes of the He-NH_3 mixture under similar conditions.

Diffuse reflectance UV-Vis. spectra of the powder samples were recorded on a Thermoscientific Evolution-600 spectrometer. $BaSO_4$ (spectral grade) was used as a reference material. XPS measurements were carried out using a multi-probe system (Omicron Nanotechnology, Germany) equipped with a dual Mg/Al X-ray source and a hemispherical analyzer operating in constant analyzer energy (CAE) mode. The spectra were obtained with 50 eV pass energy for survey scan and 20 eV for individual scans. The Mg Kα X-ray source was operated at 300 W and 15 kV. The base pressure in the analyzing chamber was maintained at $1x10^{-10}$ mbar. The data were processed with the Casa XPS program (Casa Software Ltd., U.K.). The peak areas were determined by integration employing a Shirley-type background. Peaks were considered to be a mix of Gaussian and Lorentzian functions in a 70/30 ratio. The peaks were calibrated by taking the adventitious carbon's C 1s line as 284.9 eV. Fourier transform infrared (FT-IR) spectra for the samples were recorded using a Bruker Tensor-27 instrument.

2.3. Transesterification of vegetable oils

The catalytic activity of the samples was evaluated in a SS batch reactor (Parr, USA; 300 ml) at different run durations (2-10 h) and at different temperatures (393 – 453 K) using 1 g of finely ground catalyst (passing through ASTM 200 Mesh). The amount of oil used was 20 g; the amount of methanol used depended on the required oil/methanol mole ratio. The stirring speed for all the runs was maintained at 600 rpm. At the end of the desired reaction time, the autoclave was cooled to room temperature, the product was diluted with water (100 ml), and the catalyst was removed by filtration. The two liquid layers were separated using a separating funnel, the lower layer consisting of water, glycerol and methanol and the upper one containing fatty acid alkyl esters, unreacted oil and intermediate products.

2.4. Product analysis

The product composition was determined by analyzing the oil layer in a gas chromatograph (Perkin-Elmer Clarus 500) equipped with a FID detector using a high temperature metallic capillary column (PDMS; 6m x 0.53mm, 1μm film thickness).

Conversion and selectivity values are expressed as wt % in all the tables and figures.

3. Results and Discussion

3.1. Physicochemical properties

3.1.1. Surface area and acidity

Table 2 Textural properties and acidity of the samples.

Sample	Spinel Content (%)	S_{BET} (m^2/g)	Pore volume (ml/g)[a] [av. Pore size; nm][b]	Acidity[c] (μmol/g) (350 - 800 K)
$ZnAl_2O_4$	100.0	62	0.22 [12]	138.7
$ZnFe_2O_4$	100.0	12	0.10 [21]	40.3
ZnO	-	29	0.10 [15]	69.6
γ- Al_2O_3	-	168	0.35 [8]	626.6
5ZnAl	11.3	133	0.40 [12]	465.5
10ZnAl	22.5	116	0.36 [12]	385.8
20ZnAl	45.0	99	0.30 [12]	292.0
α-Fe_2O_3	-	6	0.06 [40]	21.1
5ZnFe	14.8	7	0.06 [34]	24.4
10ZnFe	29.6	10	0.08 [32]	27.8
20ZnFe	59.2	11	0.10 [32]	28.6

[a]: From N_2 adsorption at liquid N_2 temperature, $p/p_o = 0.98$; [b]: by BJH method; [c]: μmoles of NH_3 desorbed/g of sample in the range, 350 - 800 K.

Surface area and acidity of the various oxides and mixed oxides including the two spinels, $ZnAl_2O_4$ and $ZnFe_2O_4$ are presented in Table 2. The surface areas of mixtures of Al_2O_3 and ZnO after calcination at 873 K are smaller than those expected for physical mixtures of Al_2O_3 and ZnO. In fact, they are slightly closer to the values expected for mixtures of Al_2O_3 and $ZnAl_2O_4$ suggesting that ZnO and Al_2O_3 have reacted to form $ZnAl_2O_4$ spinel and the mixtures are probably $ZnAl_2O_4$ supported on Al_2O_3. In the case of $ZnFe_2O_4$ it is difficult to analyze the data with reasonable accuracy due to the small areas involved. Even so, the values are close to those expected for mixtures of Fe_2O_3 and $ZnFe_2O_4$. XRD results (Section **3.1.2**) also confirm the formation of $ZnAl_2O_4$ and $ZnFe_2O_4$ in the mixtures.

The pores in $ZnAl_2O_4$ are broadened compared to γ-Al_2O_3 support with increasing Zn loading in the ZnO-Al_2O_3 system (Table 2). The pore volume/size values of Fe_2O_3 suggest that it has almost a flat surface. But increasing ZnO loading creates broad pores in the ZnO-Fe_2O_3 system. ZnO has an intermediate pore distribution between $ZnAl_2O_4$ and $ZnFe_2O_4$.

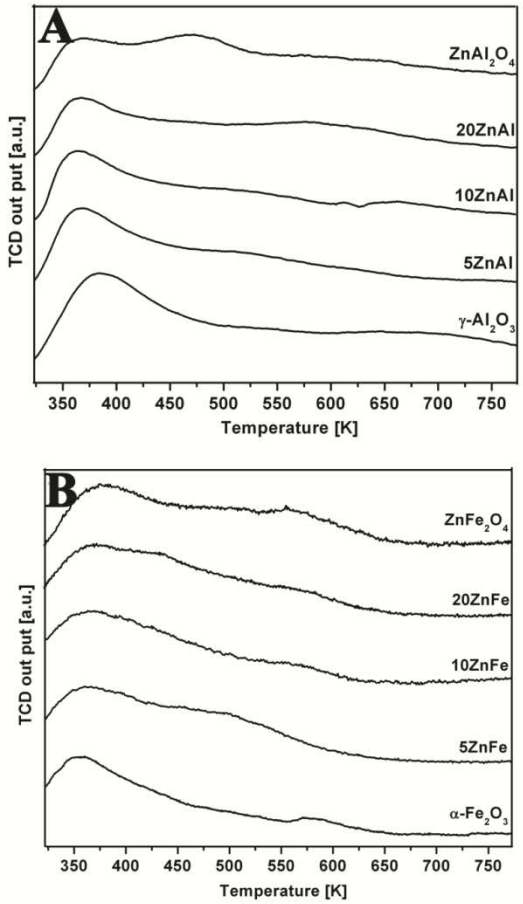

Figure 1. NH_3-TPD of A) ZnO-Al_2O_3 with different ZnO loadings and $ZnAl_2O_4$; and B) ZnO-Fe_2O_3 with different ZnO loadings and $ZnFe_2O_4$.

The acidities of the samples as measured by TPD of NH_3 are also presented in Table 2. In order to understand the acidity characteristics of the samples better, the contributions from physical adsorption (if any) and from very weak acid sites (NH_3 desorbing below 350 K) were excluded and the amount of NH_3 that desorbed in the temperature range of 350 – 800 K is presented in the last column of Table 2. The acidities of $ZnAl_2O_4$, $ZnFe_2O_4$ are 139 and 40 meq/g. The acidities of the supports, γ-Al_2O_3, Fe_2O_3 and ZnO are 627, 21 and 40 meq/g, respectively. Though the acidity of $ZnAl_2O_4$ decreases drastically compared to γ-Al_2O_3, $ZnAl_2O_4$ contains almost equal distribution of medium (peak at ~375 K) and strong (peak at ~475 K) acidic sites (Fig. 1.). But in γ-Al_2O_3, medium acidic sites are dominant than the strong acidic sites. The acidities of the supported samples are intermediate to those of the oxides and ZnO); acidity decreases in the case of Al_2O_3 and increases in the case of Fe_2O_3 with increasing ZnO loading. The less than proportionate change in acidity of the supports with ZnO loading suggests that ZnO has interacted strongly with the supports and the supported samples are not physical mixtures of the two oxides.

3.1.2. Powder X-ray diffraction

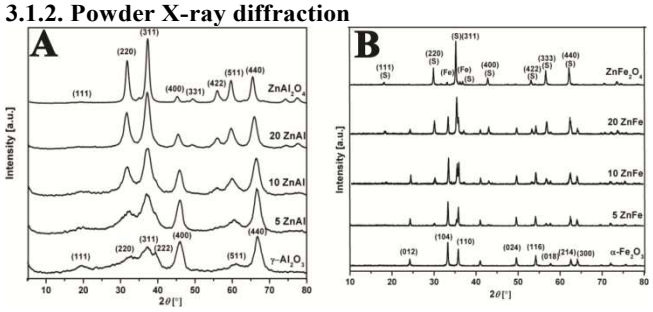

Figure 2. XRD patterns of A) ZnO-Al_2O_3 with different ZnO loadings and $ZnAl_2O_4$; and B) ZnO-Fe_2O_3 with different ZnO loadings and $ZnFe_2O_4$.

The XRD-patterns of supported ZnO (5 to 20 wt% of ZnO) samples prepared by impregnation of $Zn(NO_3)_2$ on γ-Al_2O_3 and Fe_2O_3 and calcination at 873 K are presented in Figure 1. γ-Alumina exhibits a diffraction pattern with broad, diffuse lines, typical of a microcrystalline material. With progressively increasing loading of ZnO, the lines due to γ-Al_2O_3 decrease in intensity along with a corresponding increase in the intensity of the spinel phase. A similar behavior is also seen in the patterns of the Fe_2O_3 supported ZnO samples (Fig. 1 B). The XRD patterns of $ZnAl_2O_4$ and $ZnFe_2O_4$ are typical of the expected spinel phases and are in agreement with JCPDS data (78-1601 and 86-2267). All the diffraction peaks matched well with the reported patterns. Lines due to individual oxides were barely discernible in the patterns.

3.1.3. UV-Vis spectroscopy

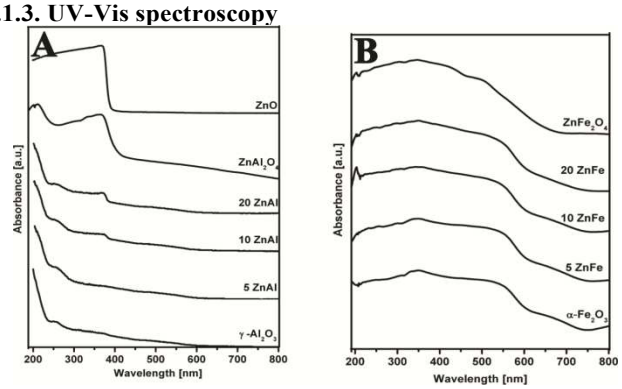

Figure 3. UV-visible spectra of A) ZnO, Al_2O_3, ZnO-Al_2O_3 samples and $ZnAl_2O_4$, and B) Fe_2O_3, ZnO-Fe_2O_3 samples and $ZnFe_2O_4$.

Table 3 Assignement of the major bands in UV-vis. spectra (Fig. 3) of spinels and oxides

Sample	Absorption maxima[a] (nm)	Assignment/Geometry	Reference(s)
$ZnAl_2O_4$	215 - 225(s) ~360	Filled O2p orbitals → empty Al3s orbitals Filled O2p→empty Zn4s orbitals (due to defects)	[34,35]
$ZnFe_2O_4$	~275,~360(b) 400-700 (b)	Ligand to metal and L→M charge transfer for Oh Fe^{3+}	[36]
Al_2O_3	215-225(b)	Filled O2p orbitals → empty Al3s orbitals	[34,35]
Fe_2O_3	250(b) ~350, ~500 and ~550	O^{2-} to Fe^{3+} charge transfer Metal to metal charge transfer	[36]
ZnO	200-400(b)	Filled O2p→empty Zn4s orbitals	[34,35]

[a]: Letters in brackets refer to nature of the absorption lines: s, strong and b, broad.

UV-vis. spectra of ZnO impregnated on Al_2O_3 and Fe_2O_3 along with those of ZnO, Al_2O_3 and Fe_2O_3 are presented in Figure 3. Assignments of the spectral bands (Figure 3) of the oxides and spinels based on published literature are presented in Table 3. Examining the spectra presented in Figure 3A, a band at ≤ 215 nm is seen for the ZnO-Al_2O_3 samples, while $ZnAl_2O_4$ exhibits a band at ~215 nm. A band noticed at ~ 250 nm in the spectra of Al_2O_3 and ZnO-Al_2O_3 samples has been attributed by earlier workers to be due to electronic excitations (O 2p → Al^{3+} 3s)[35, 36]. Additionally, with increasing Zn content, the band at ~360 nm attributed to defect Zn^{2+} sites in $ZnAl_2O_4$ is found to increase with Zn loading confirming the presence of increasing amounts of the spinel structure in the samples. The spectrum of ZnO shows a very strong and broad absorption below 380 nm with a peak maximum at ~360 nm. The similarity in the absorption band is presumably because Zn^{2+} ions in both ZnO and the spinel are both in a coordination of O^{2-} ions[35].

Increasing spinel content in the ZnO-Fe_2O_3 system does not considerably alter the absorption spectra significantly due to the broad absorption of α-Fe_2O_3 (Figure 3B) in the entire UV-visible region (the samples are brown-black). However small changes are still seen. The broad absorption at ~250 nm is due to O^{2-} → Fe^{3+} charge transfer in α-Fe_2O_3. The weak band at ~350 becomes broader and more intense with increasing Zn loading due to O^{2-} → Zn^{2+} charge transfer. Octahedral Fe^{3+} exhibits a weak band at ~500 nm due to crystal field transition which is more clearly observed in the case of $ZnFe_2O_4$ compared to other samples of the series. Intense absorption in the visible region of α-Fe_2O_3 is mainly due to various types of CT transitions like metal to metal charge transfer (MT) transitions ($2Fe^{3+}$→ Fe^{2+} + Fe^{4+}). As Zn atoms are introduced in to α-Fe_2O_3, the decrease in Fe−O−Fe linkages between adjacent Fe^{3+} cations gradually reduces the intensity of the band at ~550 nm along with increasing formation of $ZnFe_2O_4$[37].

3.1.4. X-ray photoelectron spectroscopy

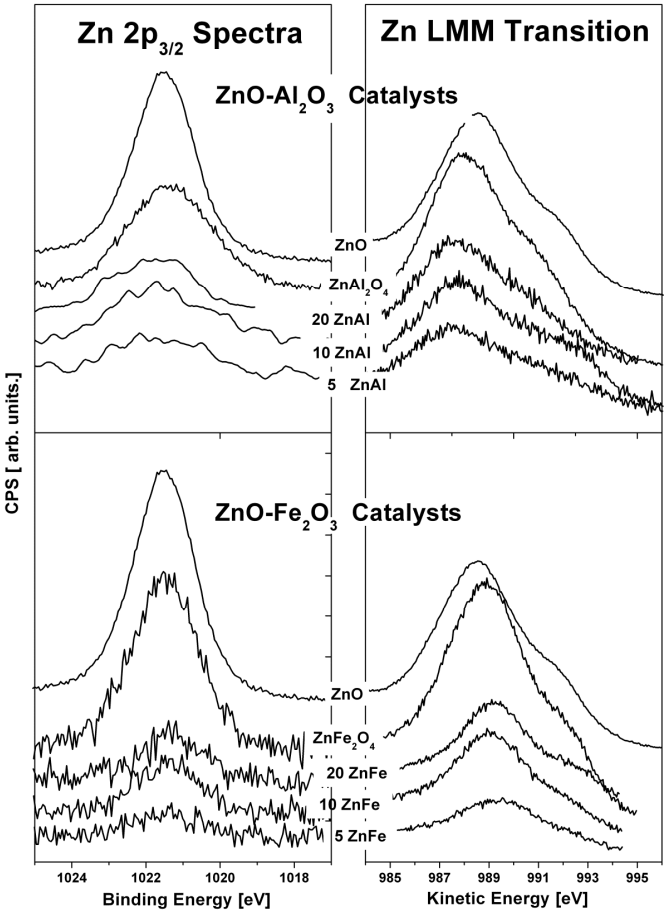

Figure 4. XP spectra of Zn $2p_{3/2}$ (left panels) and Zn LMM transitions from XAES (right panels) ZnO-Al_2O_3 and $ZnAl_2O_4$ (top panels) and ZnO-Fe_2O_3 catalysts and $ZnFe_2O_4$ (bottom panels). In top and bottom panels, XPS of Zn $2p_{3/2}$ (left panels) and XAES of Zn LMM transitions (right panels) of ZnO samples are also presented for comparison.

Table 4 Binding energies (in eV) of Zn in ZnO-Al_2O_3 and ZnO-Fe_2O_3, $ZnAl_2O_4$ and $ZnFe_2O_4$ (values in the parentheses are FWHM+ of the peaks in eV)

Sample	Zn $2p_{3/2}$[a] eV	Zn LMM[c] eV	Auger Parameter, α eV
5ZnAl	1021.0 (3.8)[b]	987.7	2008.7
10ZnAl	1021.6 (3.1)	987.8	2009.4
20ZnAl	1021.8 (2.6)	987.8	2009.6
$ZnAl_2O_4$	1021.4 (2.7)	987.9	2009.3
ZnO	1021.5 (2.0)	988.5	2010.0
5ZnFe	1021.5 (2.3)	989.2	2010.7
10ZnFe	1021.4 (2.0)	989.2	2010.6
20ZnFe	1021.3 (2.1)	989.2	2010.5
$ZnFe_2O_4$	1021.4 (2.0)	989.0	2010.4

[a]: Binding energy; [b]: Full width at half maximum; [c]: Kinetic energy.

X-ray photoelectron spectroscopy (XPS) was used to further investigate $ZnAl_2O_4$, $ZnFe_2O_4$, and samples of ZnO-Al_2O_3 and ZnO-Fe_2O_3 with different ZnO loadings. Zn $2p_{3/2}$ core level (XPS) and Zn LMM transitions (XAES) of ZnO-Al_2O_3 and ZnO-Fe_2O_3 samples are presented in Figure 4. Though the 2p core level binding energy (BE) of Zn is insensitive to differentiate the chemical states, its modified Auger parameter (α) derived from Zn $2p_{3/2}$ BE and Zn LMM Auger lines differentiates Zn^{2+} and Zn^0 states[37]. From table 4, α values of all the catalysts prepared come around ~2009±1 eV characteristic of Zn^{2+} ions[38]. The Full width at half maximum (FWHM) value for Zn $2p_{3/2}$ peak of ZnO is the least due to an unique –O–Zn– environment compared to all the catalysts presented in table 4 and therefore, in the other catalysts, Zn^{2+} ions should be present in spinel or supported spinel phase where different environments around Zn are possible as evidenced with XRD results (Section **3.1.1.**). With increasing loading of ZnO in both the systems, the difference in environment vanishes till it reaches stoichiometric spinel composition. Moreover, at lower loadings of ZnO, the spinels might be present as smaller crystallites and this may be the reason for the higher FWHM values. Zn LMM transition is observed at the kinetic energy of 987.8±0.1 eV for ZnO-Al_2O_3, at 989.0±0.1 eV for ZnO-Fe_2O_3 and 988.5 eV for ZnO. The higher value for ZnO-Fe_2O_3 shows that Zn^{2+} ions in the ferrite are richer in electrons than in the aluminates and ZnO. A shoulder in the Zn LMM transition at ~991 eV for ZnO-Al_2O_3 samples and ~992 eV for ZnO-Fe_2O_3 samples is found to emerge with increasing Zn loading in both the systems. Strohmeier and Hercules[32] have suggested that this is due to l-s coupling of the Zn atom in oxide environment. The l-s coupling is strong in case of ZnO than other catalysts.

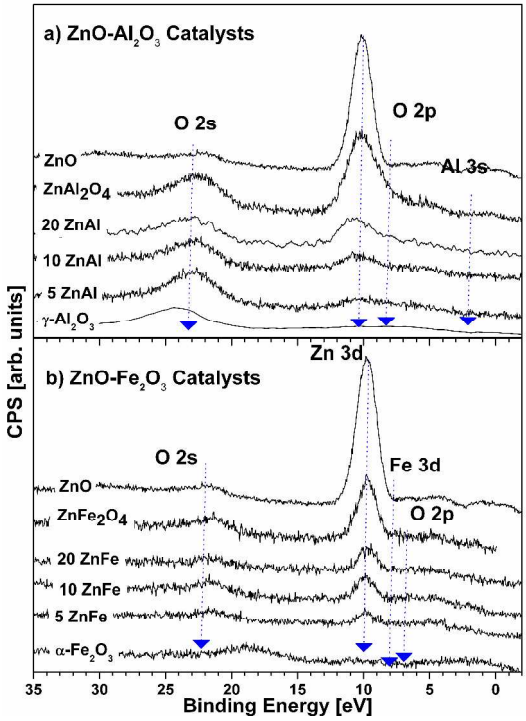

Figure 5. Valence band (VB) spectra from XPS studies of a) ZnO-Al_2O_3 and b) ZnO-Fe_2O_3 samples with corresponding stoichiometric spinels. VB spectra of γ- Al_2O_3 and Fe_2O_3 have been rescaled (÷ 10) to fit in the figure.

XP spectra in the valence band (VB) region of the ZnO-Al_2O_3 and ZnO-Fe_2O_3 samples are presented in Figure 5. The main VB appearing at 11 eV and 10 eV, respectively, in the top and bottom panels in the figure is associated with Zn 3d; the Zn 3d band of ZnO appears at 10.3 eV. Note that LMM Auger transition of Zn involves Zn 3d (L) and Zn 2p (M) electrons. In ZnO systems, the lowest valence band lies below the Zn 3d level.38 Other bands at 7eV in the top panel and 8 eV in both the panels are due to Fe 3d and O 2p levels16. Particularly, Fe 3d band appears to be very weak in all the catalysts of ZnO-Fe_2O_3 system including α-Fe_2O_3 probably due to the spin-forbidden transition of Fe^{3+} ions d5 configuration. The band for O 2s orbital appears at ~23 eV for ZnO-Al_2O_3 samples and at ~22 eV for ZnO-Fe_2O_3 samples. The higher binding energy of O 2s band of ZnO-Al_2O_3 compared to ZnO-Fe_2O_3 is due to the greater ionic nature of Al-O bonds than Fe-O bonds[40-42]. From the XVB spectra it is clear that the surface valence band is dominated by the Zn 3d orbitals in both the systems and the intensity of the Zn 3d peak increases with increasing Zn content in both the systems. From the valence band spectra, it is concluded that Zn 3d electrons are actively involved in the spinel formation for both the systems and likely to take part to a major extent in the electronic excitation of the spinels ($ZnAl_2O_4$ and $ZnFe_2O_4$) and, presumably, their catalytic activity.

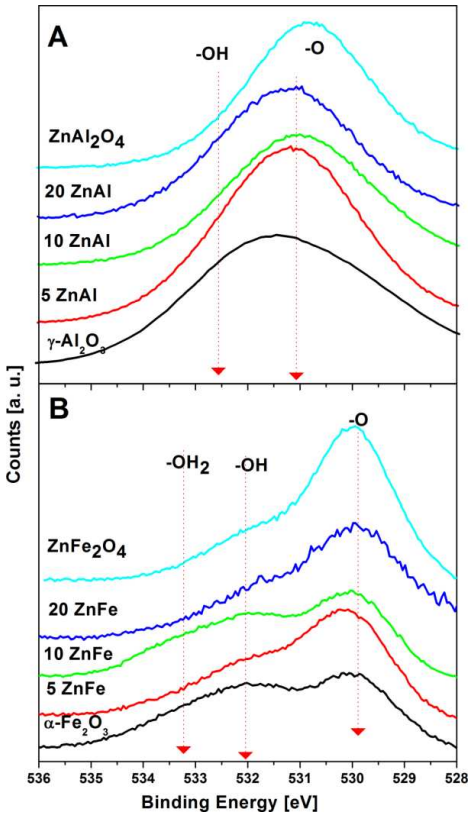

Figure 6. O 1s spectra from XPS studies of A) ZnO-Al_2O_3 and B) ZnO-Fe_2O_3 samples with corresponding stoichiometric spinels. O 1s spectrum of ZnO is also given in the figure for comparison.

XP spectra of O 1s region of ZnO/Al_2O_3 and ZnO/Fe_2O_3 samples are presented in Figure 6. At Zn loadings up to 20%, O 1s peak is observed at 531.2±0.2 eV for ZnO/Al_2O_3 and at 530±0.2 eV for Zn/Fe_2O_3 samples. O 1s peak of adsorbed water ($–OH_2$) and basic hydroxide (–OH) generally observed at 533.2±0.1 eV and 532.2±0.1 eV, respectively[43,44], are also seen in the spectra (Figure 6B).

These peaks are, however, relatively less intense in ZnO/Al_2O_3 samples and it might probably due to relatively small BE difference between the basic hydroxide group with the main O 1s peak of support Al_2O_3. From Figure 6B, it is clear that the intensity of peaks due to adsorbed water and basic hydroxide group decreases as the spinel phase is increasing. It might be due to the hydrophobic nature of the stoichiometric spinels.

3.1.5. IR Spectroscopy in DRIFTS mode

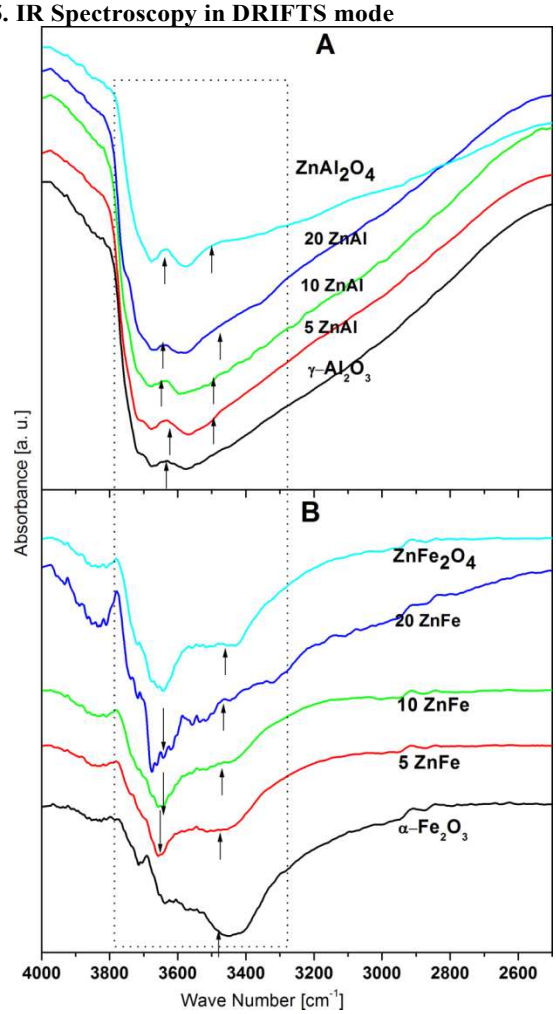

Figure 7. DRIFT IR spectra of A) ZnO, Al_2O_3, ZnO-Al_2O_3 samples and $ZnAl_2O_4$, and B) Fe_2O_3, ZnO-Al_2O_3 samples and $ZnFe_2O_4$.

The IR spectra in DRIFT mode for spinels were recorded at a sample temperature of 673 K under nitrogen atmosphere in order to avoid the interference of -OH vibrations due to moisture and presented in Figure 7. As the evolution of spinel phase with increasing ZnO loading could be clearly observed XRD, UV-Vis and XPS spectra, we concentrate in the –OH group region (4000-3000 cm^{-1}) of the IR spectra to understand the nature of surface hydroxyl groups in the spinel-type oxides in the present study. For γ-Al_2O_3 (Figure 7A), three distinct bands were observed around 3728, 3678 and 3560 cm^{-1} respectively in the "–OH" region. The first peak corresponds to terminal –OH group mainly located on octahedrally

coordinated Al^{3+} and the other two distinct bands were assigned for bridging –OH and triply-bridging –OH[45]. A new band appeared at ~3680 cm^{-1} ($ZnAl_2O_4$) must be due to the hydroxyl group on tetrahedrally coordinated Zn^{2+} with increase in Zn wt% loading on alumina[46]. However, a new band forming at 3580 cm^{-1} because of the merging of bands at 3678 and 3560 cm^{-1} might be attributed to the formation of Zn containing spinels and new bridging group Zn-O-Al surface. In the case of Fe_2O_3, IR spectra in Figure 7B exhibit multiple bands due to different types of –OH groups. The bands at 3660 and 3675 cm^{-1} are attributed to the hydroxyl groups on octahedral Fe^{3+}. A weak band at ~3719 cm^{-1} is observed for the terminal –OH group which lies on tetrahedral Fe^{3+} either non vacant or near cation vacancy for pure Fe_2O_3[46]. The bands for bridging and triply bridging –OH group appear at ~3550 cm^{-1} and at ~3450 cm^{-1} (a broad peak) respectivly[46]. Similar to $ZnAl_2O_4$ samples, the intensity of the band at ~3680 cm^{-1} increases with increasing ZnO content as the result of newly formed –OH groups on tetrahedral Zn^{2+}. Consequently, in $ZnAl_2O_4$ and $ZnFe_2O_4$, the intensity of the various hydroxyl groups decreases with increase in the ZnO percentage i.e formation of spinel phase. This indicates the formation of new hydrophobic sites on the spinel type oxide surface.

3.2. Studies on transesterification of vegetable oils

Evaluation of the catalytic activity of the different ZnO loaded Al_2O_3 and Fe_2O_3 samples in the transesterification of vegetable oils with methanol was carried out in a SS batch reactor using the three different vegetable oils, sunflower, and jatropha and waste oils.

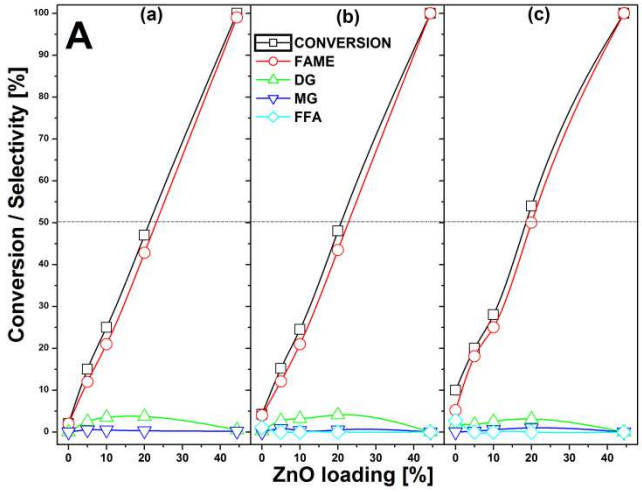

.

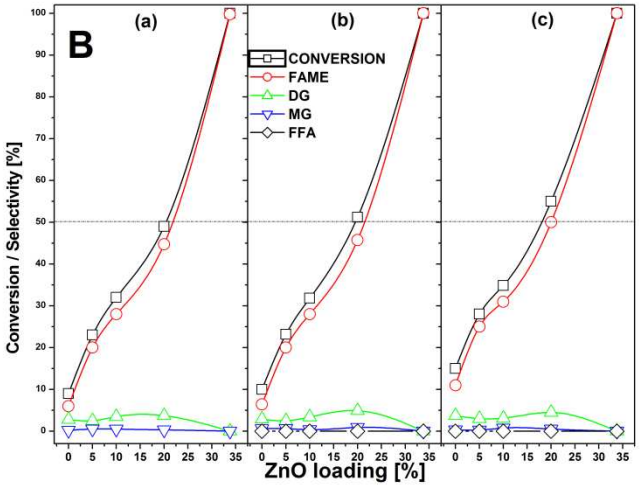

Figure 8. Influence of ZnO loading on transesterification activity of [A] ZnO/Al_2O_3 samples: a) sunflower oil, b) waste cooking oil and c) jatropa oil (conditions: catalyst, 1 g; 453 K; oil, 20 g; MeOH/oil (mole), 9; run duration, 10 h). [B] ZnO/Fe_2O_3 samples: a) sunflower oil, b) waste cooking oil and c) jatropa oil (conditions: catalyst, 1 g; 453 K; oil, 20 g; MeOH/oil (mole), 9; run duration, 10 h).

The transesterification activities of the supported spinel catalysts are given in Figure 8. Conversion of sunflower oil (triglycerides, TG) and the individual selectivity for the intermediates, the di and monoglycerides (DG and MG), and the final product FAME are presented in the figures as a function of % ZnO loading. The last point in the figures is for the stoichiometric spinel prepared by the coprecipitation method. It is seen that activity increases linearly with ZnO content, the linearity being more in the case of ZnO-Fe_2O_3 samples. In the case of the pure spinels, the (nearly) only product of the reaction is the mixture of fatty acid methyl esters (FAME). The other expected products, viz. the diglycerides (DG) and monoglycerides (MG) were together less than 0.5 wt% in the product. More of these intermediates, especially the MG, are found in the case of the less active samples. Even so, the amounts of these compounds are less than 4 % in all the products. It appears from these studies that Zn spinel phase is mainly responsible for activity of these calcined mixed oxides. The imaginary lines drawn in figure 8 clearly indicate that the transesterification activity is better for 5, 10 and 20 % loadings of ZnO of ZnO-Fe_2O_3 samples than ZnO-Al_2O_3 samples. Both the catalysts can be used for at least 5 cycles without noticeable loss in activity and can be used for fixed bed run for at least 48 hrs, according to our present study. The detailed results of the transesterification activity studies on $ZnFe_2O_4$ spinel catalyst with other spinel catalysts is discussed elsewhere[33].

3.3. Structure-Activity Correlations

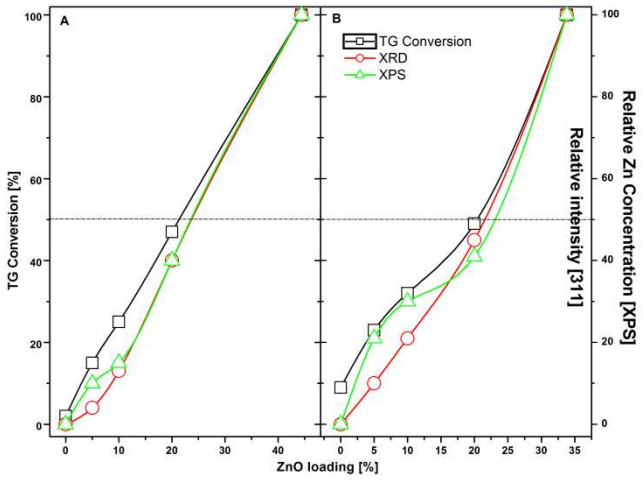

Figure 9. Relationships between ZnO loading, transesterification activity, relative spinel-content from XRD peak (311) intensity and relative intensity of Zn 2p peak in XPS for A) ZnO-Al_2O_3 and B) ZnO-Fe_2O_3 (conditions: catalyst, 1 g; 453 K; sunflower oil, 20 g; MeOH/oil (mole), 9; run duration, 10 h).

Characterization studies reported earlier revealed the formation of spinel-type phases in the samples, making them essentially spinels supported on Al_2O_3 and Fe_2O_3. XRD studies revealed the formation of increasing amounts of the spinel species with increasing Zn-loading, while UV-vis. and XPS studies also provided indirect evidence for the formation of the spinel phases. The information on the surface hydroxyl groups of the mixed spinel-type oxides in the present study with XPS (O 1s region) and DRIFT-IR studies reveals the creation of hydrophobic sites with increasing ZnO content. Indeed, these hydrophobic sites facilitate the rapid adsorption of TG, which is also hydrophobic[47].

Plots of amount of Zn loaded in ZnO-Al_2O_3 and ZnO-Fe_2O_3 samples vs. their catalytic activity, relative bulk spinel content (as established by intensity of 311 peak in XRD) and relative intensity of Zn 2p measured by XPS are presented in Figure 9. Nearly linear relationships between Zn-loading, spinel-content, surface Zn-intensity (XPS) and activity (sunflower oil conversion) are noticed (Figure 9) confirming the role of the spinel phase in catalytic activity. Relative intensity values (XRD and XPS) were calculated with respect to the stoichiometric spinels prepared by the co-precipitation method (the last point in the figures). In case of ZnO-Fe_2O_3 samples relative surface Zn concentrations from XPS closely follow the transesterification activity than ZnO-Al_2O_3 samples, suggesting direct involvement of spinel phase to the activity in the former compared to the later. From the characterization studies, it is clear that ZnO-Al_2O_3 catalysts are highly porous with high surface area and ZnO-Fe_2O_3 catalysts are almost flat with low surface area. Therefore more transesterification activity of ZnO-Al_2O_3 catalysts than the surface Zn concentrations must be due to the higher surface area and porous nature of them; on the other hand, the activity of ZnO-Fe_2O_3 catalysts can be attributed to the surface concentrations of Zn^{2+} ions.

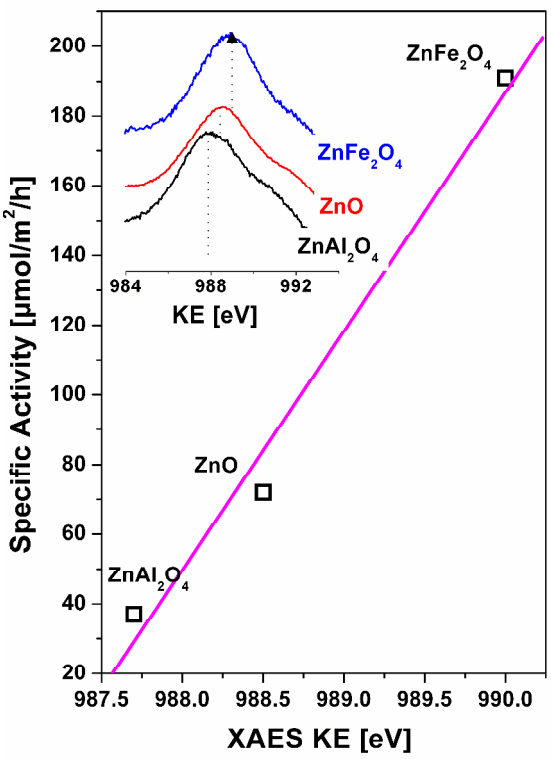

Figure 10. The linear relationship of Zn LMM (XAES) transitions with the specific transesterification activities of $ZnAl_2O_4$, ZnO and $ZnFe_2O_4$. The inset shows the corresponding Zn LMM transitions of $ZnAl_2O_4$, ZnO and $ZnFe_2O_4$.

Table 5 Comparison of activity of different spinels and oxides.

Sample	Surface area[a] (m^2/g)	Acidity µmol/g (350 - 800 K)	Activity (% conversion) at run time		Specific activity[b] (µmol/m^2/h) at run time	
			10 h	2 h	10 h	2 h
$ZnAl_2O_4$	62	138.7	100	20	35	37
$ZnFe_2O_4$	12	40.3	100	21	190	191
ZnO	29	69.6	98	17	79	72
γ-Al_2O_3	168	626.6	2	-	0.2	-
α-Fe_2O_3	6	21.1	9	2	33	38

[a]:From N_2 adsorption, using BET equation; [b]:TG converted per mol per unit surface area per gram of catalyst (conditions: catalyst, 1 g; 453 K; sunflower oil, 20 g ; MeOH/oil (mole), 9.

The activity of the different oxides and the two spinels are compared (on wt and area basis) in Table 5. The conversions recorded on the two spinels, $ZnAl_2O_4$ and $ZnFe_2O_4$, at a run time of 10 h are similar, being about 100%. However, their activities are different when they are calculated on area basis. There is no direct relationship with surface area and acidity with the transesterification activity as can be seen in Table 5. Comparing the specific activities calculated on surface area basis at a run time of 2 h, it is found that $ZnFe_2O_4$ is much more active (191 µmol/m^2/h) than $ZnAl_2O_4$ (37 µmol/m^2/h). Though the activity of ZnO is also fairly large (72 µmol/m^2/h), it is,

however, found to leach into the reaction medium during, and hence not suitable as a catalyst. It is interesting to point out here that the specific activities of $ZnAl_2O_4$, $ZnFe_2O_4$ and ZnO for transesterification reaction increase in the same order of Zn LMM values, i.e., the electron density on Zn^{2+} ions. ($ZnAl_2O_4$ (987.7±0.1 eV) < ZnO (988.5 eV) < $ZnFe_2O_4$ (990±0.1 eV), Section **3.1.4.**) (see, Figure 10). The activity of the pure oxides are much lower, sunflower oil conversion being 9 and 2 % at 10 h, respectively, over Fe_2O_3 and Al_2O_3, though due to the low surface area of Fe_2O_3, its specific activity is, however, large (35 μmol/m^2/h).

Activation energy values based on biodiesel conversion gave an E_a value of 14.5 kCal/mole for $ZnAl_2O_4$ and 14 kCal/mole for $ZnFe_2O_4$ for sunflower oil (Figure S1, in supplementary information) suggesting the absence of diffusion effects at the experimental conditions used. Similar values have been reported by earlier workers during acid catalyzed transesterification of vegetable oils[48]. This further proves that the $ZnFe_2O_4$ surface considerably reduces the activation energy of the reaction than $ZnAl_2O_4$ even though it has a flat surface and lower surface area but electron rich Zn-ions.

4. Conclusions

The studies reveal that when $Zn(NO_3)_2$ is impregnated on Al_2O_3 and Fe_2O_3 and calcined at 873 K, crystalline spinel phases of $ZnAl_2O_4$ and $ZnFe_2O_4$ are readily formed on the surface. Both $ZnAl_2O_4$ and $ZnFe_2O_4$ are active in the tranesterification of vegetable oils (sunflower, jatropa and waste cooking oils). A linear relationship between Zn-spinel content and transesterification activity is obtained for the supported catalysts. XVB (x-ray valence band) studies reveal that the surface valence bands of the two spinels are dominated by the Zn 3d orbitals and the intensity of the Zn 3d peak increases with increasing Zn content in the supported samples; this suggests that Zn 3d electrons are likely to take part to a major extent in the electronic excitation of the spinels ($ZnAl_2O_4$ and $ZnFe_2O_4$) during the reaction and, presumably, their transesterification activity. The electron densities of Zn-ions play a crucial role in the activity of the examined spinel samples.

Acknowledgements

The authors thank Head, NCCR, IIT Madras and DST, New Delhi.

Notes and references

[a] *National Centre for Catalysis Research, Indian Institute of Technology, Chennai-600 036. India.*
Tel. 044-22574238
E-mail:KThirunavukkarasu@gmail.com (Dr. K. Thirunavukkarasu)
[b]*Department of Chemistry*
Anna University
Chennai – 600 025. India.

Electronic Supplementary Information (ESI) available: [details of any supplementary information available should be included here]. See DOI: 10.1039/b000000x/

1 Z. Helwani, M.R. Othman, N. Aziz, J. Kim, W.J.N. Fernando, *Appl. Catal. A: Gen*., 2009, **363**, 1-10.
2 M. Di Serio, R. Tesser, L. Pengmei, E. Santacesaria, *Energ. Fuel*, 2008, **22**, 207-217.
3 G.R. Peterson,W.P. Scarrah, *J. Am. Oil. Chem. Soc*., 1984, **61**, 1593-1597.
4 E. Lotero, Y. Liu, D.E. Lopez, K. Suwannakaran, D.A. Bruce, J.G. Goodwin, Jr., *Ind. Eng. Chem. Res*., 2005, **44**, 5353-5363.
5 D.-W. Lee, Y.-M. Park, K.-W. Lee, *Catal. Surv. Asia*, 2009, **13**, 63-77.
6 R. Stern, G. Hillion, J.-J. Rouxel, S. Leporq, US Patent 5908946, 1999, to Institut Francais du Petrole.
7 L. Bournay, G. Hillion, P. Boucot, J.-A. Chodorge, C. Bronner, A. Forestiere, US Patent 6878837, 2005, to Institut Francais du Petrole.
8 W.R. Cares, J.W. Hightower, *J. Catal*., 1971, **23**, 193-203.
9 F. L. Peltier, P. Chaumette, J. Saussey, M. M. Bettahar, J. C. Lavalley, *J. Mol. Catal. A: Chem.*, 1998, **132**, 91-100.
10 R. Roesky, J. Weiguny, H. Bestgen, U. Dingerdissen, *Appl. Catal. A: Gen*., 1996, **176**, 213-220.
11 H. Grobowska, W. Mista, J. Trawczycz, M. Zawadzki, *Appl. Catal. A: Gen*., 2001, **220**, 207-213.
12 T. E. Nabarawy, A. A. Attia, M. N. Alaya, *Mater. Lett*., 1995, **24**, 319-325.
13 G. Aguilar-Rios, M. Valenzuela, P. Salals, M. Armendariz, P. Bosh, G. Del Toro, R. Silva, V. Bertin, S. Castillo, A. Ramirez-soliz, I. Schiftler, *Appl. Catal. A: Gen*., 1995, **127**, 65-75.
14 X. Li, Z. Zhu, Q. Zhao, L. Wang, *J. Hazard. Mater*., 2011, **186**, 2089-2096.
15 L. Zhang, J. Yan, M. Zhou, Y. Yang, Y-N. Liu, *Appl. Surf. Sci*.,, 2013, **268**, 237-245.
16 M. Vijayaraj, C. S. Gopinath, *J. Catal*., 2006, **241**, 83-95.
17 K. Sreekumar, S. Sugunan, *Appl. Catal. A: Gen*, 2002, **230**, 245-251.
18 P.T.A. Santos, A.C.F. Costa, H.M.C. Andrade, *Mater. Sci. Forum*, 2012, **727-728**, 1290-1295.
19 F.M. Moghadden, M. Doulabi, H. Saeidian, *Sci. Iranica C*, 2012, **19**, 1597-1600.
20 H. Lee, J. C Jung, H. Kim, Y-M. Chung, T. J. Kim, S. J. Lee, S-H. Oh, Y. S. Kim, I. K. Song, *Catal. Lett*., 2009, **131**, 344-349.
21 H. Armendariz, G. Aguilar-Rios, P. Salas, M.A. Valenzuala, Schifter, H. Arrioka, N. Nava, *Appl. Catal. A: General*, 1992, **92**, 29-38.
22 Dom, R., Subasri, R., Hebalkar, N.Y., Chary, A.S., Borse, A.S., *RSC Adv*., 2012, **2**, 12782-12791.
23 G.Fan, J. Tong, F. Li, F., *Ind. Eng. Chem. Res*., 2012, **51**, 13639-13647.
24 X. Xu, A.K. Azad, J.T.S. Irvine, *Catal. Today*, 2013, **199**, 22-26.
25 J-P. Jacobs, A. Maltha, J. G. H. Reintjes, J. Drimal, V. Ponec, H. Brongersma, *J. Catal*., 1994, **147**, 294-300.
26 N. Nava,J. P. Jacobs, A. Garcla, J. J. W. M. Rosink, M. A. Valenzuela, L. J. Van Ijzendoorn, H. H. Brongersma, J. Radioanal. Nucl. *Chem. Lett*., 1996, **212**, 431-443.
27 L. Bournay, D. Casanave, B. Delfort, G. Hillion, J.A. Chodorge, *Catal.Today*, 2005, **106**, 190-192.
28 V. Pugnet, S. Maury, V. Coupard, A. Dandeu, A-A. Quoineaud, J-L. Bonneau, D. Tichit, *Appl. Catal. A: Gen.*, 2010, **374**, 71-78.
29 W. Jiang, H-F. Lu, T .Qi, S-I.Yan, B. Liang, *Biotechnol. Adv*., 2010, **28**, 620-627.

30 Q. Liu, L. Wang, C. Wang, W. Qu, Z. Tian, H. Ma, D. Wang, B. Wang, Z. Xu, *Appl. Catal. B: Environ.*, 2013, **136– 137**, 210– 217.
31 C. T. Alves, A. Oliveira, S. A. V. Carneiro, A. G. Silva, H. M .C. Andrade, S. A. B Vieira de Melo, E. A. Torres, *Fuel Processing Technology*, 2013, **106**, 102-107.
32 B. R. Strohmeier, D. M. Hercules, *J. Catal*., 1984, **86**, 266-279.
33 T.M. Sankaranarayanan, A. Pandurangan, M. Banu, S. Sivasanker, *Appl. Catal. A: Gen*., 2011, **409-410**, 239-247.
34 T.M. Sankaranarayanana, R. Vijaya Shanthi, K. Thirunavukkarasu, A. Pandurangan, S. Sivasanker, *J. Mol. Catal. A: Chemical*, 2013, **379**, 234-242.
35 S. K. Sampath, J. F. Cordaro, *J. Am. Ceram. Soc*., 1998, **81**, 649 – 654.
36 S. Mathur, M. Veith, M. Haas, H. Shen, N. Lecerf, V. Huch, S. Hufner, R. Haberkorn, H.P. Beck., *J. Am. Ceram. Soc*., 2001, **84**, 1921-1928.
37 L.G.J. de Haart, G. Blasse, *J. Electrochem. Soc*., 1985, **132**, 2933-2938.
38 G. Moretti, J. Electron Spectrosc. Related Phenom., 1998, **95**, 95-144.
39 L Ley, R. A. Pollak, F. R. McFecly, S. I'. Kowalczyk, D. A. Shirley, *Phys. Rev. B*, 1974, **9**, 600-621.
40 R.H. French, *J. Am. Ceram. Soc*., 1990, **73**, 471-489.
41 Y. Yourdshahyan, C. Ruberto, M. Halvarsson, L. Bengtsson, V. Langer, B.I. Lundqvist, *J. Am. Ceram. Soc*., 1999, **82**, 1365–1380.
42 G. Rollmann, A. Rohrbach, P. Entel, J. Hafner,. *Phys. Rev. B: Condens. Mater*., 2004, **69**, 165107-165119.
43 K. Kotsis, V. Staemmler, *Phys. Chem. Chem. Phys.*, 2006**, 8**, 1490-1498.
44 J.L. Junta-Rosso, M.F. Hochella Jr., *Geochim. Cosmochim. Acta*. 1996, **60**, 305-314.
45 A.A. Tsyganenko, K.S. Smirnov, A.M. Rzhevskij, P.P. Mardilovich, *Mater. Chem. Phys.*, 1990, **26**, 35-46.
46 G. Busca, V. Lorenzelli, G. Ramis, R.J. Willey, *Langmuir,* 1993, **9**, 1492-1499.
47 D.M. Reinoso, D.E. Damiani, G.M. Tonetto, *Appl. Catal. B: Environ.* 2014, **144**, 308– 316.
48 B.Freedman, R.O.Butterfield, E.H.Pryde, *J. Am. Oil Chem. Soc*.,1986, **63**, 1375-1380.